2-D Time-Dependent Viscoelastic Flow Calculations Using CONNFFESSIT

Manuel Laso
Dept. of Chemical Engineering, ETSII, E-28006 Madrid, Spain

Marco Picasso
Dept. of Mathematics, Ecole Polytechnique Féderal de Lausanne, CH-1015 Lausanne, Switzerland

Hans Christian Öttinger
ETH Zürich, Dept. of Materials, Institute of Polymers, CH-8092 Zürich, Switzerland

Two-dimensional time-dependent calculations for a molecular model of finite extensibility in the journal-bearing geometry are presented. The flow is considered to be incompressible and isothermal. The momentum conservation equation is integrated using a time-marching procedure in which local ensembles of dumbbells act as stress calculators. The calculations are based on the Calculation of non-Newtonian flows: finite elements and stochastic simulation technique (CONNFFESSIT) and combine deterministic (finite elements) and stochastic techniques to advance the velocity and stress fields in time. The ability of CONNFFESSIT to treat models for which no closed-form constitutive equation can be derived is illustrated by performing calculations using FENE dumbbells. Significant differences in the stress field between the true FENE and the linearized FENE-P are found, especially during the inception period. Steady-state kinematics are, however, identical within error bars for both FENE and FENE-P and for the Newtonian fluid. The essential algorithm of 2-D CONNFFESSIT is detailed, as well as experience gathered from its parallel and vector versions.

Introduction

Since it was first proposed (Öttinger and Laso, 1992) the viability of the calculation of non-Newtonian flows: finite elements and stochastic simulation technique (CONNFFESSIT) for the calculation of viscoelastic flows has been demonstrated for one-dimensional (1-D) time-dependent (Laso and Öttinger, 1993a,b) and two-dimensional (2-D) steady-state flows (Feigl et al., 1994, 1995). The latter calculations were performed in a contraction flow for the Oldroyd-B constitutive equation by sending ensembles of Hookean dumbbells along streamlines and averaging their contributions to the stress in each element. Although this procedure leads to correct results for steady-state calculations, it is not the most direct way to perform a 2-D CONNFFESSIT calculation. This article presents a more natural method for 2-D time-dependent flows that closely resembles the flow of real polymer molecules in solution or in the melt. The ability to treat molecular models for which no closed-form constitutive equation exists is demonstrated by performing calculations for the finitely extensible nonlinear elastic (FENE) model.

Correspondence concerning this article should be addressed to M. Laso.

Molecular Models and Constitutive Equation

The FENE model was first proposed for dumbbells as an attempt to improve the Hookean dumbbell by including finite molecular extensibility (Warner, 1972; Bird et al., 1987).

A FENE fluid consists of a suspension of neutrally buoyant noninteracting dumbbells in a Newtonian fluid. The restoring force of the spring follows a nonlinear law and grows without bound as the elongation approaches a critical value. At small elongation, there is little deviation from the Hookean behav-

ior; as the elongation approaches the maximum, the restoring force grows without bound. Since real polymer molecules deviate from Gaussian behavior as their elongation approaches the maximum chain extensibility (i.e., all-trans in a linear alkane), the finite extensibility of the FENE model makes it somewhat more realistic than the Hookean dumbbell.

The force law for the FENE model is given by

$$F^C = \frac{HQ}{1-\left(\frac{Q}{Q_0}\right)^2}. \tag{1}$$

An analytically tractable dumbbell model can be obtained by replacing the configuration-dependent nonlinear factor in the FENE spring law by a self-consistently averaged term (Peterlin, 1961, 1962):

$$F^C = \frac{HQ}{1-\left\langle\frac{Q^2}{Q_0^2}\right\rangle}, \tag{2}$$

where the angle brackets imply an ensemble average value.

Still other approximations have been proposed, including hydrodynamic interaction and nonconstant diffusion coefficient for the beads (Chilcott and Rallison, 1988; Öttinger, 1987; Wedgewood and Öttinger, 1988; Wedgewood et al., 1991). For a detailed evaluation of several FENE models, see Herrchen and Öttinger (1996). In this work we limited ourselves to the FENE and FENE-P models. These dumbbell models can be characterized by three constants: the first, $\lambda = \zeta/4H$, is a characteristic relaxation time, similar to the one defined for Hookean dumbbells, and the second is the dimensionless finite extensibility parameter

$$b = \frac{HQ_0^2}{kT},$$

which can be interpreted as the (dimensionless) maximum elongation squared. Although from the mathematical point of view the value of b could be chosen at will, it must remain within a certain range if physical meaning is to be attached to it. Typical values for vinyl polymers are in the range of 30 to 300 (Herrchen and Öttinger, 1996). The third constant α specifies what fraction of the total viscosity of the polymer solution at zero shear rate is due to the Newtonian solvent:

$$\alpha = \frac{\eta_s}{\eta_s + \eta_p^0}.$$

Whereas the kinetic theory of some microscopic models for polymer dynamics can be solved analytically to yield a macroscopic constitutive equation (CE), for the FENE fluid such an expression can be found only for steady state and only up to cubic terms in the velocity gradient (Bird et al., 1987). Lacking a CE, traditional continuum-mechanical methods are unable to calculate the behavior of a polymeric fluid described by a FENE model under general nonhomogeneous flow.

The linearized FENE-P model leads to a closed-form analytical CE (Bird et al., 1987, Eqs. 13.5-56) of considerable complexity for numerical viscoelastic flow calculations. Although it was used by Mochimaru to solve the startup of planar Couette flow (Mochimaru, 1983), it has only recently started to be used in complex geometries (Purnode, 1996). While the static behavior of the linear FENE-P model is fairly close to that of the FENE, its dynamic behavior for the inception of plane shear flow and simple elongational flow is notably different (Herrchen and Öttinger, 1996; Laso and Öttinger, 1993a). The rheological properties of FENE chains, in comparison with various approximations, has been investigated via BD simulation by van den Brule (1993).

Two-Dimensional CONNFFESSIT

As in most viscoelastic flow calculations, the objective of a CONNFFESSIT calculation is to solve the equations of mass and momentum conservation for an incompressible, isothermal non-Newtonian fluid:

$$(\nabla\cdot v) = 0$$

$$\rho\frac{\partial v}{\partial t} + [\nabla\cdot\rho vv] + [\nabla\cdot\pi] = 0,$$

where π is the total momentum-flux or total stress tensor that can be split in the following way:

$$\pi = p\delta + \tau.$$

This set of partial differential equations must be closed by a third equation (the CE) relating τ to the history of the flow.

In a CONNFFESSIT calculation, the fundamental difficulty associated with kinetic models for which no closed-form CE can be derived is bypassed, since all that is required is a consistent microscopic model, even if its kinetic theory is analytically unsolvable. The contribution of the polymer to the stress is obtained from a stochastic simulation of a suitable molecular model (elastic or rigid dumbbells, bead-spring-rod chains, reptation models, etc.).

These molecules act as stress computers that can be used in a standard method based on a discretization of the domain like finite elements: all molecules located in a given element (or subelement) contribute to the stress of that element (see Eqs. 18 and 19 below). Molecules are entrained by the macroscopic flow of the fluid, much as happens in real polymer solutions or melts. In the simplest case, the centers of mass of the molecules follow streamlines, that is, in our 2-D calculations for FENE or FENE-P, the components of the position vector of the center of mass of a given dumbbell obey the equations:

$$\frac{dx}{dt} = v_x(t,x,y) \tag{3}$$

$$\frac{dy}{dt} = v_y(t,x,y). \tag{4}$$

The dynamics of the internal degrees of freedom of the dumbbell are described by stochastic differential equations

which can be derived from the diffusion equation in configuration space or can be postulated on physical grounds. A description of the correspondence between Fokker-Planck equations and stochastic differential equations can be found in Öttinger (1996). For elastic dumbbells in the absence of external forces, the diffusion equation in configuration space can be written as (Bird et al., 1987):

$$\frac{\partial \psi}{\partial t} = \frac{2}{\zeta}\left(\frac{\partial}{\partial \boldsymbol{Q}} \cdot \boldsymbol{F}^{C}\psi\right) - \left(\frac{\partial}{\partial \boldsymbol{Q}} \cdot [\boldsymbol{\kappa} \cdot \boldsymbol{Q}]\psi\right) + \frac{2kT}{\zeta}\left(\frac{\partial}{\partial \boldsymbol{Q}} \cdot \frac{\partial}{\partial \boldsymbol{Q}}\psi\right).$$

This equation is formally a Fokker-Planck equation (Risken, 1989) that has its counterpart in a stochastic differential equation (SDE), which for the force law of Eq. 1 has the form

$$d\boldsymbol{Q} = \left\{[\boldsymbol{\kappa} \cdot \boldsymbol{Q}] - \frac{2H}{\zeta} \frac{\boldsymbol{Q}}{1 - \left(\frac{\boldsymbol{Q}}{Q_0}\right)^2}\right\} dt + \sqrt{\frac{4kT}{\zeta}}\, d\boldsymbol{w}, \quad (5)$$

where $\boldsymbol{w}$ is a 3-D Wiener process, and similarly for Eq. 2.

Equation 5 can be made dimensionless by dividing by $\sqrt{kT/H}$ and using the definition of λ:

$$d\boldsymbol{Q}' = \left([\boldsymbol{\kappa} \cdot \boldsymbol{Q}'] - \frac{1}{2\lambda} \frac{\boldsymbol{Q}'}{1 - \frac{\boldsymbol{Q}'^2}{b}}\right) dt + \sqrt{\frac{1}{\lambda}}\, d\boldsymbol{w}. \quad (6)$$

And similarly for the FENE-P fluid, that is, force law given by Eq. 2:

$$d\boldsymbol{Q}' = \left([\boldsymbol{\kappa} \cdot \boldsymbol{Q}'] - \frac{1}{2\lambda} \frac{\boldsymbol{Q}'}{1 - \frac{\langle \boldsymbol{Q}'^2 \rangle}{b}}\right) dt + \sqrt{\frac{1}{\lambda}}\, d\boldsymbol{w}. \quad (7)$$

These SDEs fully describe the dynamics of the polymer molecules and give a physical interpretation of the mechanisms intervening: the first term in the parenthesis corresponds to the deterministic effect of the underlying macroscopic flow of the solvent, which tends to rotate and extend the dumbbell; the second term represents the restoring force of the spring; and the last term corresponds to the Brownian agitation to which the dumbbells are subjected due to bombardment by solvent molecules.

Equations 6 (for FENE) and 7 (for FENE-P) contain all the dynamic information required to perform the stochastic calculation for a given starting configurational distribution; for example, at equilibrium ($\boldsymbol{\kappa} = \mathbf{0}$), the distribution of the connector vector $\boldsymbol{Q}'$ for FENE dumbbells is

$$\psi(\boldsymbol{Q}') = \frac{1}{2\pi b^{3/2} B\left(\frac{3}{2}, \frac{b+2}{2}\right)} \left[1 - \frac{\boldsymbol{Q}'^2}{b}\right]^{b/2}, \quad (8)$$

for $(\boldsymbol{Q}')^2 < b$, and 0 otherwise.

For FENE-P dumbbells at equilibrium,

$$\psi(\boldsymbol{Q}') = \frac{1}{(2\pi)^{3/2}[\det(\boldsymbol{\sigma})]^{1/2}} \exp\left(-\frac{1}{2}\boldsymbol{Q}' \cdot \boldsymbol{\sigma}^{-1} \cdot \boldsymbol{Q}'\right), \quad (9)$$

where the covariance matrix,

$$\boldsymbol{\sigma} = \frac{b}{b+3}\boldsymbol{\delta}.$$

In the second step of CONNFFESSIT, the contribution of the polymer molecules to the stress tensor for a given ensemble of dumbbells is evaluated using Kramer's form for the polymer contribution to the stress in terms of the normalized connector vector:

$$\boldsymbol{\tau}_p = -nkT\left(\left\langle \frac{\boldsymbol{Q}'\boldsymbol{Q}'}{1 - \frac{\boldsymbol{Q}'^2}{b}} \right\rangle - \boldsymbol{\delta}\right) \quad \text{(FENE)} \quad (10)$$

$$\boldsymbol{\tau}_p = -nkT\left(\frac{\langle \boldsymbol{Q}'\boldsymbol{Q}' \rangle}{1 - \frac{\langle \boldsymbol{Q}'^2 \rangle}{b}} - \boldsymbol{\delta}\right) \quad \text{(FENE-P)}. \quad (11)$$

In a CONNFFESSIT calculation, Eqs. 6, 7, 10 and 11 are valid for the local ensembles (of size N^j_{loc}) in each element j. Assuming the fluid to be initially at rest, the ensembles are initialized by distributing the total number of dumbbells in the global ensemble (N_g) over all elements with a uniform density of dumbbells, the configurations ($\boldsymbol{Q}'$), which are drawn from the corresponding equilibrium distributions, Eqs. 8 for FENE, and 9 for FENE-P. The initial conditions define the velocity field (possibly zero everywhere), and therefore the velocity gradient at $t = 0$, both of which are used to advance the position of the centers of mass and of the internal degrees of freedom of the dumbbells by a small time interval (the first step $\Delta t_1 = t_1 - t_0$ in a partition of time into intervals $[t_i, t_{i+1})$, where $t_i < t_{i+1}$, $i = 0, 1, 2, \ldots$). After this step, the stress in each element (or in a suitable subelement) is computed using Eqs. 10 and 11 and used as a constant term or body force in the integration of the equation of momentum:

$$\rho\frac{\partial \boldsymbol{v}}{\partial t} + \rho(\boldsymbol{v} \cdot \nabla)\boldsymbol{v} - 2\eta_s \nabla \cdot (\nabla \boldsymbol{v} + (\nabla \boldsymbol{v})^T) + (-\bar{z})\nabla(\nabla \cdot \boldsymbol{v}) = -\nabla \cdot \boldsymbol{\tau}^p, \quad (12)$$

where the contribution to the stress of the Newtonian suspending fluid has been written explicitly. Additionally, the in-

compressibility condition has been replaced with the penalty equation:

$$p = -\bar{z}(\nabla \cdot \boldsymbol{v}),$$

where $\bar{z}$ is a large penalty parameter (typically 10^8). The fluid is thus treated as being slightly compressible. This is a popular method for solving incompressible fluid problems since it eliminates not only the incompressibility condition but also pressure as an unknown.

In the present work, the three types of integrations required in a 2-D CONNFFESSIT calculation were performed in the following way:

1. Integration of the trajectories of the centers of mass of the dumbbells.

Except in a few special cases (Öttinger, 1992), most existing models for polymer dynamics assume that the center of mass of a dumbbell follows streamlines. This is the case for both the FENE and the FENE-P models. Since the velocity field is known at all times, determining dumbbell paths is a straightforward problem. We have integrated the trajectories of the centers of mass of the dumbbells using an explicit first-order Euler method:

$$x_{i+1}^j = x_i^j + v_x(x_i^j, y_i^j, t_i)\Delta t_i \tag{13}$$

$$y_{i+1}^j = y_i^j + v_y(x_i^j, y_i^j, t_i)\Delta t_i, \tag{14}$$

while in planar flow the z-component is ignored. Higher-order algorithms were not required for sufficiently accurate integration in the smooth geometry of the journal bearing for the time steps used.

A close correspondence exists between the integration of dumbbell paths and the tracking of upstream trajectories in traditional viscoelastic flow calculations with integral constitutive equations (Luo and Tanner, 1986; Malkus and Bernstein, 1984; Viriayuthakorn and Caswell, 1980). In CONNFFESSIT, particle tracking closely mimics the flow of real polymer molecules. Determination of transit times through elements and integration over flow histories are carried out automatically by the flowing dumbbells: all required information about the history of the flow is contained in their instantaneous configurations.

2. Integration of the internal degrees of freedom of the dumbbells.

Integration of Eq. 6 (FENE) was performed using the following semi-implicit second-order algorithm (Öttinger, 1996), in which the spring-force law is treated explicitly in the predictor step and implicitly in the corrector step:

$$\bar{\boldsymbol{Q}}'^j(t_{i+1}) = \boldsymbol{Q}'^j(t_i) + \left[\boldsymbol{\kappa}(t_i)\cdot\boldsymbol{Q}'^j(t_i) - \frac{1}{2\lambda}\frac{\boldsymbol{Q}'^j(t_i)}{1-\dfrac{(\boldsymbol{Q}'^j(t_i))^2}{b}}\right]\Delta t_i + \sqrt{\frac{\Delta t_i}{\lambda}}\,\boldsymbol{W}_i^j. \tag{15}$$

$\bar{\boldsymbol{Q}}'^j(t_{i+1})$ is subsequently corrected by

$$\left[1+\frac{1}{4\lambda}\frac{\Delta t_i}{1-\dfrac{(\boldsymbol{Q}'^j)^2(t_{i+1})}{b}}\right]\boldsymbol{Q}'^j(t_{i+1}) = \boldsymbol{Q}'^j(t_i) + \frac{1}{2}\left[\boldsymbol{\kappa}(t_{i+1})\cdot\bar{\boldsymbol{Q}}'^j(t_{i+1}) + \boldsymbol{\kappa}(t_i)\cdot\boldsymbol{Q}'^j(t_i) - \frac{1}{2\lambda}\frac{\boldsymbol{Q}'^j(t_i)}{1-\dfrac{(\boldsymbol{Q}'^j(t_i))^2}{b}}\right]\Delta t_i + \sqrt{\frac{\Delta t_i}{\lambda}}\,\boldsymbol{W}_i^j, \tag{16}$$

where the same random numbers $\boldsymbol{W}_i^j$ occur in Eq. 15 and Eq. 16. The direction of $\boldsymbol{Q}'^j(t_{i+1})$ is given by the direction of the righthand side of Eq. 16, and its length can be determined from a cubic equation which, for arbitrary length of the vector on the righthand side of Eq. 16, has a single root between 0 and $\sqrt{b}$.

This predictor–corrector scheme requires the velocity gradient at t_{i+1} to be known at t_i. This is the case in the simulation of rheological homogeneous flows, but not in viscoelastic flow calculations in complex geometries. In a naive application of the PC scheme, Eq. 15 would be evaluated first, followed by an integration step of the equation of motion (in order to obtain $\boldsymbol{\kappa}(t_{i+1})$), by the corrector step Eq. 16 and by a repetition of the integration step of the equation of motion. This procedure is, however, not satisfactory since the predicted value of $(\bar{\boldsymbol{Q}}'^j(t_{i+1}))^2$ may be unphysically large ($> b$) for some j. Furthermore, it requires the storage of $3N_g$ random deviates (which is a very large number) between the evaluation of Eq. 15 and Eq. 16, since $\boldsymbol{W}_i^j$ must be the same for the predictor and the corrector steps. A proper way of applying the previous PC scheme in a CONNFFESSIT calculation is to approximate $\boldsymbol{\kappa}(t_{i+1})$ in Eq. 16, for example, by a backwards difference formula:

$$\bar{\boldsymbol{\kappa}}(t_{i+1}) = \boldsymbol{\kappa}(t_i) + \dot{\boldsymbol{\kappa}}(t_i)\Delta t_i \approx \boldsymbol{\kappa}(t_i) + \left(\frac{\boldsymbol{\kappa}(t_i)-\boldsymbol{\kappa}(t_{i-1})}{\Delta t_{i-1}}\right)\Delta t_i$$

and then to apply Eqs. 15 and 16 in succession for each dumbbell without intermediate updates of the velocity field.

FENE-P dynamics (Eq. 7) were integrated using an explicit Euler scheme:

$$\boldsymbol{Q}'^j(t_{i+1}) = \left(\left[\boldsymbol{\kappa}(t_i)\cdot\boldsymbol{Q}'^j(t_i)\right] - \frac{1}{2\lambda}\frac{\boldsymbol{Q}'^j(t_i)}{\left(1-\dfrac{1}{bN_{\mathrm{loc}}^j}\sum_k(\boldsymbol{Q}'^k(t_i))^2\right)}\right)\Delta t + \sqrt{\frac{\Delta t}{\lambda}}\,\boldsymbol{W}_i^j, \tag{17}$$

where the index k runs over the indices of the dumbbells belonging to the jth element (jth local ensemble).

3. Integration of the momentum conservation equation.

The integration of Eq. 12 was performed by a standard semi-implicit time-marching finite-element technique. In the present work, bilinear, quadrilateral finite elements were used so that the velocity was continuous across two quadrilateral elements. Quadrilaterals were split in two triangles within which the stress was constant, the value of the stress being assigned to the central Gaussian integration point. Although this finite element does not satisfy the *inf-sup* stability condition and is known to produce spurious checkerboard effects in the pressure (Pironneau, 1989), it is widely used because of its simplicity and because the velocity field (in which we are mainly interested) can be obtained accurately and is not subject to artifacts. The resulting system of equations was solved by a direct method.

The experience gained up to now seems to indicate that even simpler elements (like simple continuous linear triangular finite elements) may be more computationally advantageous, although this equation deserves systematic quantitative evaluation.

Time marching was performed by means of a scheme implicit in the velocity and explicit in the polymer contribution to the stress, that is, the polymer contribution to the stress was treated as a righthand-side constant at each step. This stress is computed with regard to an element (or possibly a subelement) as a local ensemble average. For the FENE model:

$$\tau_p^j(t_i) = nkT\left[\frac{1}{N_{\text{loc}}^j}\left(\sum_k \frac{Q'^k(t_i)Q'^k(t_i)}{1-\dfrac{(Q'^k(t_i))^2}{b}}\right) - \delta\right] \quad \text{(FENE)} \tag{18}$$

and for the FENE-P model:

$$\tau_p^j(t_i) = nkT\left[\left(\frac{\dfrac{1}{N_{\text{loc}}^j}\displaystyle\sum_k Q'^k(t_i)Q'^k(t_i)}{1-\dfrac{1}{bN_{\text{loc}}^j}\displaystyle\sum_k (Q'^k(t_i))^2}\right) - \delta\right] \quad \text{(FENE-P)}, \tag{19}$$

where the counter k runs over the indices of all dumbbells belonging to the jth element (jth local ensemble).

The schemes just presented allow us to advance the microscopic stochastic simulations, the dumbbell paths, and the macroscopic conservation equations by one time step. The partition of time used to advance Eq. 12 needs not be the same as the one used for the integration of Eq. 6 and for the evaluation of the stresses (Öttinger and Laso, 1994). However, in the present work we have used the same constant time steps for all three.

Particle Tracking and Velocity-Biased Neighbor Lists

The evaluation of Eqs. 13 through 16 and of 18 (for the FENE fluid) requires the knowledge of the index of the element in which each dumbbell is located at every time step. Since dumbbells are entrained by the macroscopic flow, in the course of a simulation they move across elements according to the instantaneous velocity field. After each time step, a number of molecules will have left the elements they were located in ("lost" particles). Hence the need to perform particle (dumbbell) tracking or relocation at each step in two-dimensional CONNFFESSIT calculations. Particle tracking involves testing whether a dumbbell k is located in an element j and repeating this for all dumbbells. The majority of dumbbells will still be located in the same element. Lost particles must be relocated.

However, given the large numbers of dumbbells $N_g = O(10^5-10^7)$ and elements $N_{el} = O(10^3-10^4)$, a brute-force search of $O(N_g N_{el})$ at each time step is out of the question. Since the characteristic size (length) of an element is much larger than the typical displacement of a dumbbell in a single time step, the dumbbells that leave an element at a given time step are almost always to be found either in nearest or in second-nearest neighbors. The task of locating all dumbbells after every time step is greatly simplified if neighbor lists are generated. Particle neighbor lists are a device widely used in molecular dynamics simulations of complex fluids to speed up the calculation of interactions (Allen and Tildesley, 1987). The same idea can be applied to generate element neighbor lists (ENL). An ENL contains, for each element in the mesh, the indices of the elements that share at least one vertex (first neighbors) with the cell under consideration. Second neighbors of a given cell share at least one vertex with its first neighbors and are themselves not first neighbors. The use of an ENL makes it unnecessary to check all elements in the mesh and allows a reduction of the complexity of the localization of dumbbells from $O(N_g N_{el})$ to $O(N_g)$.

Since the velocity field is known at each step, the search can be further sped up by ordering the elements in the ENL so that those located downstream of the given cell are searched first. The natural way of implementing such a velocity-biased ENL is to sort the lists of first and second neighbors in order of increasing absolute value of the angle formed between the velocity vector at a characteristic point of the central cell (e.g., the centroid) and the vector joining the centroid of the central cell with the centroid of a neighboring cell (angle θ in Figure 1). Thus, for deterministic dumbbell trajectories, all dumbbells that have left an element will necessarily be found in downstream elements; in practice, locating a dumbbell seldom involves searching more than the first three elements of the velocity-biased ENL. A new sorting of first and second neighbors needs to be done only if major changes in the velocity field have taken place since the list was last sorted. In the present calculations, because of the very small radial component of the velocity, the initial sorting was in all cases sufficient for the whole length of the calculation. The use of a velocity-biased ENL resulted in an average reduction by a factor of 6.7 in the effort required to relocate the dumbbells with respect to a nonbiased ENL.

In spite of the speed-up afforded by a velocity-biased ENL, it is crucial that the actual decision of whether a dumbbell is located within an element or not be done efficiently since it must be repeated a very large number of times in the course of a simulation. In the present work, the following point-inclusion algorithm was used:

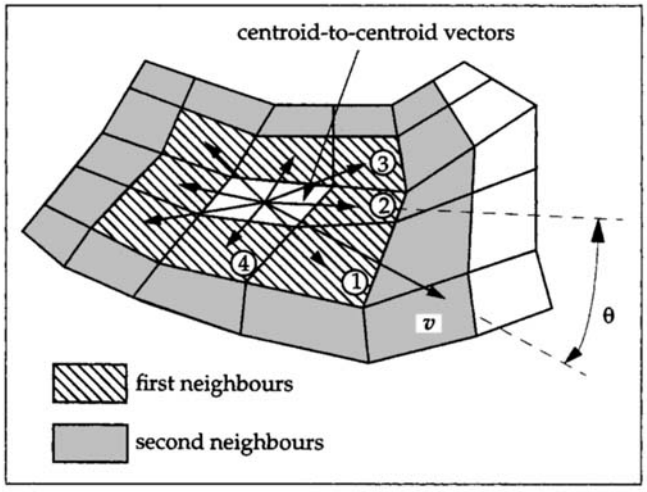

Figure 1. Velocity-biased element neighbor list (ENL).

Numbers in circles indicate the searching order in a velocity biased ENL.

Initialization (before starting the time iteration):

- For each element k, determine the coordinates of some arbitrary interior point, for example, its centroid (X_c^k, Y_c^k).
- For each side of the element, determine and store the coefficients a_i^{kj} of the Cartesian equations of the jth side $f^{kj}(a_i^{kj}, x, y) = 0$, where $j = 1, N_{\text{sides}}$ and $i = 1, N_{\text{coeff}}$. These equations are in most cases polynomials of degree one.
- Evaluate $\text{sign}(f^{kj}(a_i^{kj}, X_c^k, X_c^k))$ and store it for each of the sides of each element.

During the time iteration, in order to determine whether the lth dumbbell of coordinates (x^l, y^l) is located within the kth element, it is sufficient to evaluate $\text{sign}(f^{kj}(a_i^{kj}, x^l, y^l))$; the dumbbell is within element k if and only if $\text{sign}(f^{kj}(a_i^{kj}, x^l, y^l))$ and $\text{sign}(f^{kj}(a_i^{kj}, X_c^k, X_c^k))$ are the same for all sides of the kth element, that is, for all j.

This sequence of steps corresponds to determining whether the dumbbell in question lies on the same half-plane defined by each of the sides of the element as a known interior point, in this case the centroid.

Once the coefficients of the equations defining the sides are known (the computation of which amounts to a negligible overhead during initialization), point-inclusion in a polygonal element can be determined with at most N_{sides} multiplications, additions, and Boolean operations per dumbbell.

Basic Data Structure, Parallelization, and Vectorization

One of the most salient features of CONNFFESSIT calculations is the presence of stochastic noise in the stresses, the strength of which decreases only with the square root of the size of the ensemble. Since the noise in the stresses results in noisy velocities, usefully accurate solutions require the use of large ensembles. Hence the need to device efficient data structures that allow the exploitation of advanced computer architectures, vector, parallel or, ideally, both.

A little thought reveals the ease with which CONNFFESSIT calculations can be parallelized: since all manipulations at the molecule level (integration of internal and external degrees of freedom, relocation) and the evaluation of the stress are very local issues (they require information at the element level only), it is natural to split these calculations among several processors so that each deals with a group of elements chosen in such a way that the number of molecules per processor (node) is roughly equal; for an initially uniform spatial coverage of the domain by dumbbells, this is tantamount to splitting the domain such that all processors receive an equal share of the area or volume of the domain. Since the fluid is incompressible, the number of molecules per element remains essentially constant, except for small fluctuations. Therefore, the partitioning of elements over processors can be done at the very beginning of the calculation and does not have to be redone again. In this sense, the molecular or microscopic part of CONNFFESSIT can be said to belong to the class of embarrassingly parallel problems. Furthermore, this part of CONNFFESSIT scales well over a wide range of number of available processors.

As far as parallelization of the macroscopic part of CONNFFESSIT (the finite-element calculation) is concerned, the task is unfortunately not so simple, although great progress is being made currently (see, for example, Zone et al., 1994).

Both parts are, however, independent in the sense that the overall calculation involves performing all molecular or microscopic calculations in order to get τ^p, and then using τ^p in order to solve the macroscopic equations of conservation. Micro- and macrocalculations are performed strictly in alternation and do not interfere with each other. Communication between the two levels is achieved via the velocity field and the stress field as shown in Figure 2. Therefore, parallelization at one level is independent of parallelization at the other. Ideally, both micro- (stochastic) and macro- (finite-element) calculations should be parallelized.

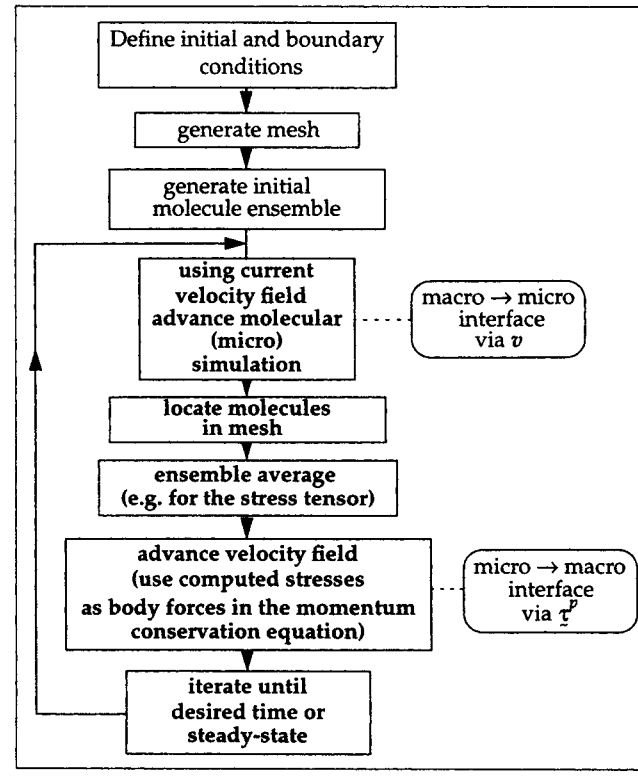

Figure 2. Basic time-marching scheme in CONNFFESSIT.

The most natural parallelization strategy in CONNFFESSIT is the element direction, rather than the molecule direction because

- It seems to make physically more sense to assign one or more elements and the particle residing in them to a given node because all molecules in a given element share the same macro information (e.g., velocity and velocity gradient).
- Ensemble averaging will almost always be performed with regard to an element; therefore the convenience of keeping together all members of the local ensembles.

However, unless special data structures are used, physically neighboring particles will in general not be neighbors in the arrays that contain their coordinates, indices, and so forth. Furthermore, relocation of particles after a time step or after a reenmeshment requires intensive interelement communication. These issues are of capital importance not only for parallelization but for vectorization as well.

Independent of the details of the molecular (stochastic) simulation, the information pertaining to individual molecules of the global ensemble (or at least pointers to that information) must be kept in a suitable kind of linear array. The organization of this indexing array has far-reaching consequences on computational efficiency and as already mentioned on vectorization and parallelization.

In this work an array sorted with regard to the elements was used to hold pointers to the individual dumbbells. In CONNFFESSIT, molecules are entrained by the macroscopic flow, and therefore cross boundaries between and move through a succession of elements. As a consequence, the labels or indices of the particles residing in a given element (the members of the local ensemble) change with time. This circumstance makes physically contiguous particles noncontiguous in the linear array containing them.

The objective of constructing an array sorted with regard to the elements is to provide indirect indexing capability, which can be used to bypass the noncontiguity problem.

It is essential for efficient vectorization to have physically neighboring molecules (i.e., molecules in the same element) placed in neighboring positions in memory. While it would be possible to initialize the positions of particles so as to ensure contiguity at the start of a calculation, the macroscopic flow would render this initial order useless at every time step. It is, however, possible to create an array sorted according to the elements that holds the indices of the particles contained in each element plus two pointer arrays that mark the start and the end of the sequence of particle indices for each element within the sorted array. The indirect addressing capability offered by the indexing array and the information contained in the pointer arrays act *de facto* as an interface that makes the particles appear as if they actually were contiguous. Fully vectorized loops over all particles in a given element are then possible, the start and end of these loops being determined by the pointer arrays. In average CONNFFESSIT calculations, the length of these loops is considerably larger than typical vector pipe lengths, thus leading to high performance.

The crucial part of this procedure is that it relies on sorting for restoring contiguity. Particle index sorting using the binary radix sort has optimal $O(N_g \log N_g)$ complexity. Besides, indirect addressing is fully supported (and in some cases hardware-executed) by all vector computers. Thus, the computational overhead associated with reordering the particle at each time step is perfectly acceptable. Since it is itself vectorizable and allows all other operations at the molecule level to be fully vectorized, the effort spent in reindexing pays back amply. A typical sustained performance on a single Cray Y-MP processor is approximately 65% of peak with an average vector length of 97.2% of the hardware vector length. The vectorized performance on this particular processor is on average 13 times higher than on a scalar MIPS R4400 at 200 MHz.

Since stochastic simulations are at the heart of the Monte Carlo method for sampling distributions, these results disprove the widespread opinion that it is impractical to vectorize Monte Carlo methods.

In all calculations, random numbers were generated using Marsaglia and Zaman's "subtract-with-borrow" algorithm (Park and Miller, 1988). For the parallel computations, the same generator was used to produce N_p seeds on the front-end host, one for each computational element, in the following way: first, a set of $10^6(N_p-1)+1$ random numbers were generated, and N_p of them were chosen equally spaced along this succession. Each of these N_p numbers were then shuffled according to the algorithm of Bays and Durham as described in Knuth (1981) and distributed over the computational nodes to be used as seeds. The same algorithm was used for vector computations: in order to obtain high performance, a number of independent copies equal to the vector length of the hardware being run simultaneously. Sustained performance of this vectorized version on one processor of the NEC SX-3 was approximately 5×10^7 uniform random deviates per CPU second. For the runs reported in the following sections, $O(10^{10})$ random numbers had to be generated.

Journal Bearing

The journal bearing has been the subject of numerous investigations, analytical, numerical, and experimental (Ballal and Rivlin, 1976; Beris et al., 1983, 1984, 1986, 1987; Burdette, 1989; Davies and Walters, 1973; Fix and Paslay, 1967; Lawler et al., 1986; Phan-Thien and Tanner, 1981; Rajagopalan, 1992; Reiner et al., 1969; Rivlin, 1979; Roberts and Walters, 1992; Sommerfeld, 1904; Tanner, 1963; Yeh et al., 1984). It consists of two nested cylinders of infinite length, the axes of which are parallel and separated by a distance e (Figure 3). The integration domain Ω is the set of points interior to the outer cylinder and exterior to the inner cylinder. The geometry of the cylinders is specified by two dimensionless parameters: the dimensionless eccentricity

$$\epsilon = \frac{e}{R_o - R_i},$$

and the dimensionless gap

$$\mu = \frac{R_o - R_i}{R_i},$$

which are written in terms of the average gap between the cylinders. Varying the eccentricity between zero and unity,

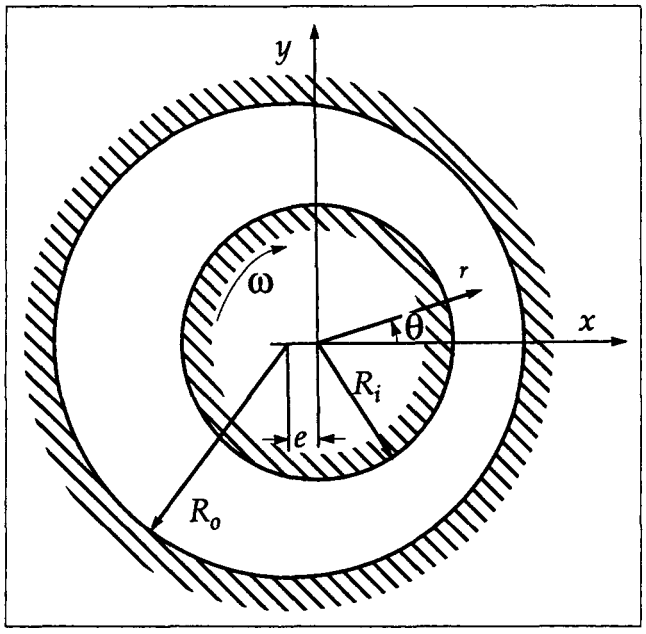

Figure 3. Geometry of journal bearing.

the flow field can be deformed from a simple shearing motion to a flow with separation. Also, the motion is nearly homogeneous shear flow when the gap parameter μ is small and $\epsilon = 0$.

The position of a point within the domain is specified either by its Cartesian coordinates (x, y), its polar coordinates (r, θ), or its normalized radial coordinate and its azimuthal angle (ξ, θ):

$$\xi = \frac{r - R_i}{(R_o - R_i)[1 - \epsilon \cos(\theta)]}.$$

The elasticity of the flow is characterized by the Weissenberg number:

$$Ws = \frac{\lambda \omega R_i}{R_o - R_i}.$$

As a typical unsteady flow, we have studied the startup problem: both cylinders and the fluid are at rest for $t < 0$ and the inner cylinder starts rotating with a constant angular velocity ω at $t = 0$, while the outer cylinder remains stationary. We further impose no-slip boundary conditions at both cylinders, that is,

$$\boldsymbol{v}(x, y) = \mathbf{0} \quad \forall (x, y) | (x, y) \in \Omega \quad \text{at} \quad t = 0 \tag{20}$$

$$\boldsymbol{v}(x, y) = \mathbf{0} \quad \text{at} \quad \xi = 1, \forall \theta \quad \text{and} \quad t > 0 \tag{21}$$

$$\boldsymbol{v}(x, y) = -R_i \omega \boldsymbol{\delta}_\theta \quad \text{at} \quad \xi = 0, \forall \theta \quad \text{and} \quad t > 0. \tag{22}$$

In order to test convergence and stability with respect to mesh refining, four increasingly finer meshes were used (the number of nodes and elements are given in Table 1). Due to the low eccentricity and gap used in most calculations, the aspect ratio of the elements was quite unfavorable, although it improved for the finer meshes. Reduced accuracy in finite-element calculations is known to be a side effect of inadequate element shape. This effect was well below the statistical noise inherent in the CONNFFESSIT calculations presented here.

Table 1. Meshes Used for the Journal-Bearing Computations

Mesh	No. of Nodes	No. of Elements	Elements in Azimuthal Direction	Elements in Radial Direction
M1	220	200	20	10
M2	476	448	28	16
M3	840	800	40	20
M4	1,680	1,600	80	20

Except where explicitly indicated, the tangential velocity of the inner cylinder, the zero-shear-rate viscosity of the fluid and the (dimensional) gap had the following values in all calculations:

$$R_i \omega = 1 \qquad \eta_s + \eta_p^0 = 1 \qquad R_o - R_i = 1.$$

Calculations at Zero Eccentricity

As a first step in the assessment of the suitability of CONNFFESSIT in 2-D calculations, several calculations were performed at zero eccentricity:

1. For the Oldroyd-B fluid constitutive equation:

$$\boldsymbol{\tau} + \lambda_1 \boldsymbol{\tau}_{(1)} = -\eta_0 (\gamma_{(1)} + \lambda_2 \gamma_{(2)}),$$

where

$$\lambda_2 = \frac{\eta_s}{\eta_s + nkT\lambda_1} \lambda_1 = \alpha \lambda_1$$

and the fluid viscosity at zero shear rate η^0 is composed of a Newtonian part $\eta_s = \alpha \eta^0$ and a polymer contribution $\eta_p^0 = (1 - \alpha)\eta^0 = nkT\lambda_1$ it is possible to obtain an exact solution to the startup problem at zero eccentricity and arbitrary gap by numerically inverting the following Laplace transform with respect to s:

$$\mathcal{L}(v_\theta(r, t)) = \frac{1}{s} \left(\frac{J_1(\bar{s}r)\Upsilon_1(\bar{s}R_i) - J_1(\bar{s}r)\Upsilon_1(\bar{s}R_i)}{J_1(\bar{s}R_o)\Upsilon_1(\bar{s}R_i) - J_1(\bar{s}R_o)\Upsilon_1(\bar{s}R_i)} \right), \tag{23}$$

where

$$\bar{s} = \sqrt{\frac{s\rho(1 + \lambda_1 s)}{\eta_0(1 + \lambda_2 s)}}$$

and J_1 and Υ_1 are Bessel functions of the first and second kind.

The same axisymmetric (1-D) problem with initial and boundary conditions Eqs. 20–22 was then solved with the full 2-D CONNFFESSIT using Hookean dumbbells ($b \to \infty$ in Eqs. 6 and 10) as the microscopic counterpart of the Oldroyd-B constitutive equation (Laso and Öttinger, 1993). Figure 4 shows the exact and CONNFFESSIT azimuthal velocity profiles. The level of stochastic noise for a single azimuthal velocity profile is indicated by the error bar on the curve for $t = 0.1$. The CONNFFESSIT curve corresponds to an average of the radial profiles at the 80 azimuthal angles, which

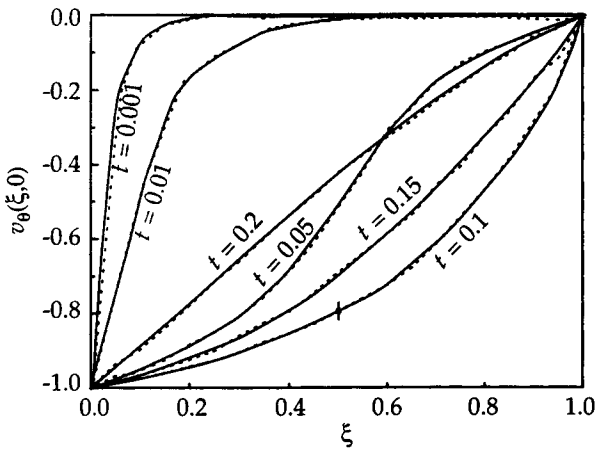

Figure 4. Startup of concentric journal-bearing flow for Oldroyd-B.

Solid line: exact solution (numerical inversion of Eq. 23); dashed line: 2-D CONNFFESSIT calculation. Mesh M4, $R_i = 2$, $\lambda_1 = 0.1$, $nkT/\rho = 80$, $\alpha = 1/9$, $N_g = 2^{19}$ dumbbells, $\Delta t = 10^{-4}$.

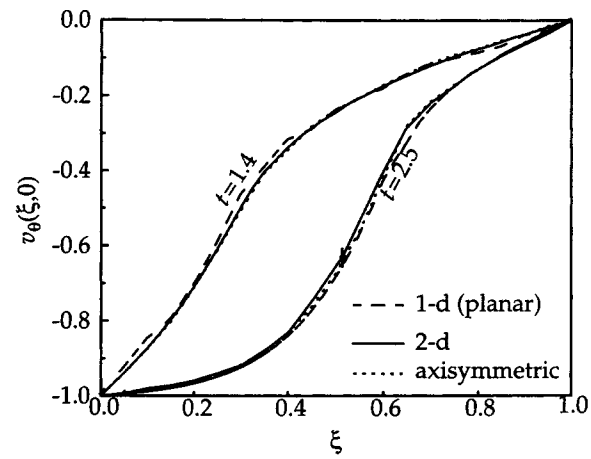

Figure 5. Azimuthal velocity profiles at $t = 1.4$ and 2.5 for startup of shear flow of FENE fluid.

Computed as a 1-D problem (plane Couette flow), as an axisymmetric problem and as a 2-D problem ($\mu = 0.1$, $\theta = 0$, $b = 50$, $\lambda = 10$, $\alpha = 0.1$, $\rho = 1$; 20 equally spaced elements and $N_g = 4 \times 10^4$ for one-dimensional and axisymmetric cases, mesh M4 and $N_g = 2 \times 10^6$ for the 2-D calculation).

must be identical by symmetry, thereby reducing the error bars by a factor of almost 9. The agreement between the analytical solution and CONNFFESSIT is very satisfactory.

2. FENE

Since there exist no analytical solutions for the flow of a FENE fluid in the journal bearing and traditional computational methods cannot provide a reference solution, it is then necessary to verify the correctness of the CONNFFESSIT calculation by indirect means.

Taking as a basis CONNFFESSIT calculations for startup of 1-D Couette flow for the FENE fluid (Laso and Öttinger, 1993), we calculated the startup of journal-bearing flow at zero eccentricity and $\mu = 0.1$. The small value of the dimensionless gap and therefore of the curvature implies that the solutions for the 1-D and the axisymmetric case must be almost identical.

In addition to the 1-D (planar) and 2-D CONNFFESSIT calculations, the same problem was solved using CONNFFESSIT in cylindrical coordinates in a manner very similar to 1-D CONNFFESSIT (Laso and Öttinger, 1993), except that the equation of momentum is

$$\rho \frac{\partial}{\partial t} v_\theta = -\frac{1}{r^2}\left(\frac{\partial}{\partial r} r^2 \tau_{r\theta}\right),$$

and the simulation of the dumbbells is now performed in cylindrical coordinates; the rotation of the frame of reference of the simulation must therefore be taken into account in the FENE dynamics, which contains an extra term with respect to Eq. 6:

$$d\boldsymbol{Q}' = \left([\boldsymbol{\kappa}\cdot\boldsymbol{Q}'] + \frac{v_\theta}{r}\begin{bmatrix} 0 & -1 & 0 \\ 1 & 0 & 0 \\ 0 & 0 & 0 \end{bmatrix}\cdot\boldsymbol{Q}' - \frac{1}{2\lambda}\frac{\boldsymbol{Q}'}{1-\frac{\boldsymbol{Q}'^2}{b}} \right) dt + \sqrt{\frac{1}{\lambda}}\, d\boldsymbol{w}$$

where $\boldsymbol{\kappa}$ is the velocity gradient in cylindrical coordinates and $\boldsymbol{Q}'$ is a column vector. The additional term is necessary because for the rigid-body rotation with angular velocity ω, the cylindrical coordinates of the connector vector $\boldsymbol{Q}'$ must remain constant and $\boldsymbol{\kappa}$ is of the form

$$\begin{bmatrix} 0 & \frac{\partial v_\theta}{\partial r} & 0 \\ -\frac{v_\theta}{r} & 0 & 0 \\ 0 & 0 & 0 \end{bmatrix}.$$

Figure 5 displays profiles of azimuthal velocity for the planar (1-D), the axisymmetric, and the 2-D (at $\theta = 0$) CONNFFESSIT calculations for meshes of the same radial resolution. The error bar for $t = 2.4$ indicates the size of the fluctuations in the 2-D CONNFFESSIT calculation. Within statistical error, the 2-D calculation faithfully reproduces the planar and axisymmetric results. The effect of the small but finite curvature is reflected in the very slight deviation between the curves for planar and axisymmetric geometries. Figure 5 shows a 2-D velocity profile at a single azimuthal angle. The 2-D velocity profile has been obtained again by averaging the radial profiles at the 80 azimuthal angles.

At larger dimensionless gaps ($\mu = 0.5$), the planar case is no longer a good approximation to the axisymmetric case, as can be seen in Figure 6. The deviation between planar and axisymmetric cases is much greater than for $\mu = 0.1$. The axisymmetric and the full 2-D calculations, however, show as good an agreement as for lower values of the dimensionless gap.

FENE and FENE-P Calculations at Low Eccentricity

Two-dimensional flow calculations for the FENE fluid in the journal-bearing geometry were performed at the same values of eccentricity ($\epsilon = 0.1$) and gap ($\mu = 0.1$) as used by

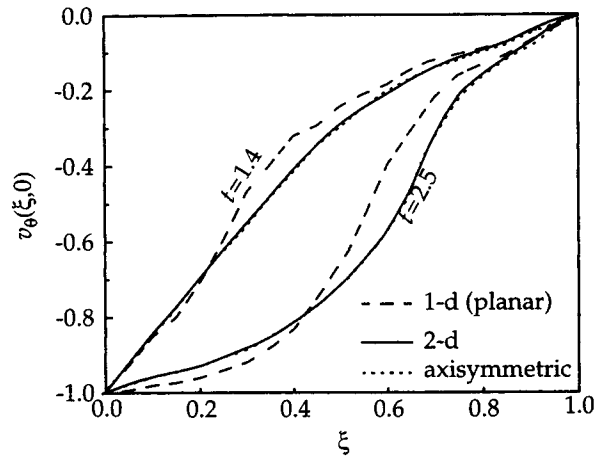

Figure 6. Same as Figure 5, but for dimensionless gap $\mu = 0.5$.

Beris et al. (1984) and at $\lambda = 3$. For this choice of parameters Ws was numerically equal to λ. The finest mesh M4 and a global ensemble of $N_g = 2^{19}$ dumbbells were used in all cases.

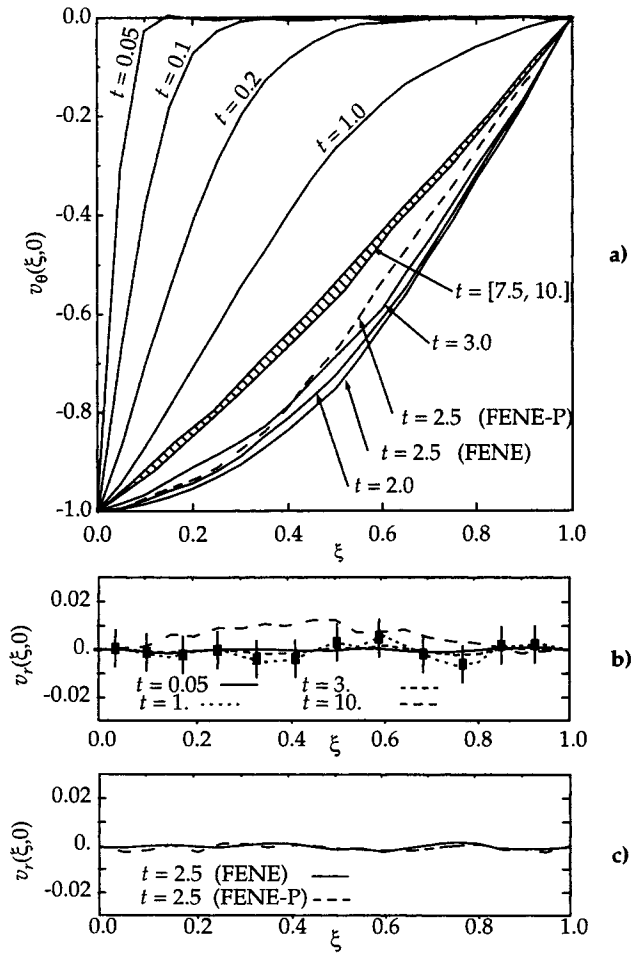

Figure 7. Radial profiles of azimuthal (a) and of radial (b) velocities for FENE and FENE-P fluids at $\theta = 0$ for $\lambda = 3$, $N_g = 2 \times 10^6$, $b = 50$, $\alpha = 0.1$, $\rho = 1$, mesh M4, $\Delta t = 0.01$; (c) radial velocities for FENE and FENE-P at $t = 2.5$.

The remaining parameters were set to $b = 50$, $\alpha = 0.1$, $\rho = 1$. All integrations were performed with a constant time step of $\Delta t = 0.01$, this value being chosen to render the round-off error of the finite-element calculation negligible in comparison with stochastic noise.

Initial and boundary conditions were Eqs. 20 and 21 and $v(0,\theta) = -\delta_\theta$ at the inner cylinder. Integration was continued up to 3λ.

Radial profiles of radial and azimuthal velocities are presented in Figure 7 (at $\theta = 0$) and Figure 8 (at $\theta = \pi$). Azimuthal velocity profiles are displayed in Figure 9. The 2-D CONNFFESSIT calculation can deliver detailed dynamic information on the evolution of the velocity field and, after sufficiently long integration, the steady-state solution. The velocity profiles contain statistical noise, which for this particular global ensemble size is of an acceptable level for the azimuthal velocities (typically, the standard deviation in the azimuthal velocity is $\sigma/|v(0,\theta)| = 0.013$ for $N_g = 2^{19}$). However, this noise level (indicated by error bars at several radial locations in Figure 7b is much too large for the radial component of the velocity to be resolved (the magnitude of which is typically 10^{-3} or about a tenth of the size of the fluctuations in the radial component of the velocity).

The steady-state velocity field is stable and in qualitative agreement with 1-D FENE calculations and 2-D calculations for several particular cases of the Giesekus fluid (Beris et al., 1984, 1986). Velocity overshoot is clearly observable. In particular the change from convex to concave in the azimuthal velocity profile at steady state as θ varies between 0 and π (mainly a consequence of mass conservation as the effective cross section of the gap increases from $\theta = 0$ and $\theta = \pi$) is accurately captured. A sigmoidal profile at $\theta = \pi$ appears af-

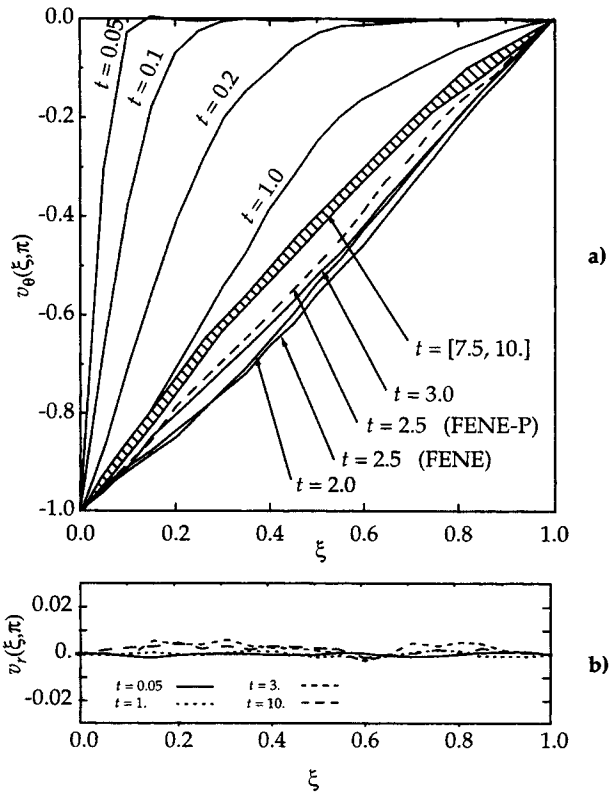

Figure 8. Same at $\theta = \pi$.

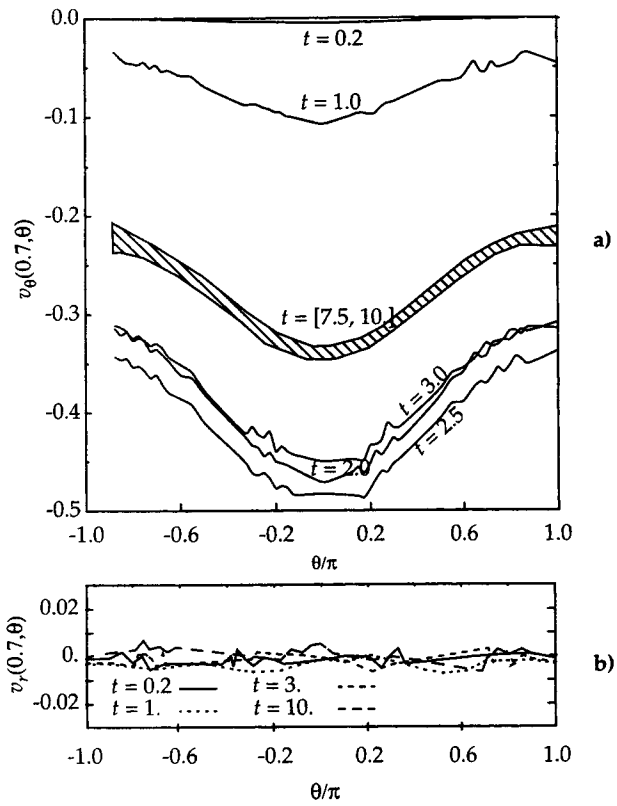

Figure 9. Azimuthal profiles of (a) azimuthal and of (b) radial velocities at $\xi = 0.7$.

ter the maximum in velocity overshoot is reached. At very short times, unphysical ($v_\theta(\xi,\theta) > 0$) azimuthal velocities at small ξ appear in both runs (e.g., profile at $t = 0.05$ in Figures 7 and 8). They are primarily due to the singularity caused by the impulsive start of the inner cylinder at $t = 0$ and are an artifact of the finite-element technique (which does not use upwinding). Additionally, the maximum in Figure 9 appears to be centered about $\theta = 0$, although the high noise level makes it impossible to discern any shift of the maximum of the expected magnitude away from $\theta = 0$ (Beris et al., 1984).

The dashed regions in Figures 7 and 8 indicate the range of fluctuation of the velocity profiles at steady state. While this accuracy can be considered satisfactory for the azimuthal velocity, the intensity of the fluctuations would preclude the observation of possible instabilities as the elasticity of the flow is increased. Such instabilities were observed by Beris et al. (1984) as regular wiggles in the radial velocity profiles with a typical relative amplitude of 10^{-4}. Achieving this level of resolution in CONNFFESSIT without resorting to variance reduction methods calls for ensemble sizes three to four orders of magnitude larger, well beyond the reach of present-day computers.

The dashed line in Figures 7a and 8a indicates the velocity profiles for the equivalent FENE-P calculation at the time at which the maximum overshoot for the FENE fluid occurs (the calculations were equivalent in the sense that all physical parameters were kept at the same values except for η_p^0, which was corrected by $(b+3)/(b+5)$). CONNFFESSIT can clearly show the difference between FENE and the more sluggish and oscillatory FENE-P response in the azimuthal velocity. Differences in the radial component lie below the stochastic noise threshold (one cannot expect CONNFFESSIT to be able to resolve such differences, since they will be of a smaller order of magnitude than the radial velocity, which is already well below the level of stochastic noise).

A further comparison of FENE and FENE-P fluids was performed in a series of calculations at the same values of eccentricity ($\epsilon = 0.1$) and gap ($\mu = 0.1$). Again mesh M4 and a global ensemble of $N_g = 2^{19}$ dumbbells were used in all cases. Figures 10 and 11 show the transient behavior of velocity and stress for the FENE and FENE-P models for $b = 50$, $\lambda = 3$, $\alpha = 0.1$, $\eta_s + \eta_p^0 = 0.1$, $\rho = 1{,}000$, $R_i = 0.1$, and $R_i\omega = 0.01$ (which correspond to a Reynolds number of 1). Integration time steps of $\Delta t = 0.01$ and 0.001 were used for FENE and FENE-P, respectively, in the CONNFFESSIT calculation. As an independent check we have included a FENE-P calculation performed with the FENE-P constitutive equation as implemented in a continuum-mechanical finite-element code (Halin et al., 1996; Purnode, 1996) using adaptive step-size. Continuum-mechanical and CONNFFESSIT calculations for the FENE-P fluid are consistent within error bars. The FENE-P model leads to a slower and more oscillatory behavior both in velocity and stress, in agreement with previous observations (Laso and Öttinger, 1993a; Herrchen and Öttinger, 1996). While the steady-state velocity is the same for both models within error bars, pronounced deviations in the stress are evident during the transient and at steady state (which sets in after a time roughly twice as long as the time required for the velocity to reach steady state).

Convergence with Mesh Refinement and Ensemble Size

To investigate the behavior of CONNFFESSIT with mesh refinement, the same flow problem for the FENE fluid was solved using meshes M1 through M4 (Table 1), keeping the size of the global ensemble (N_g) constant for all meshes. Figure 12 shows the azimuthal velocity profiles at $\theta = 0$; arrows indicate in which direction the velocity profile progresses and dashed lines correspond to overshooting velocity profiles. Curves at $t = 10$ are, within error bars, at steady state. For meshes M1 through M4, the behavior on mesh refinement is stable and the solutions are consistent within statistical noise.

Although it is conceivable that further mesh refinement could lead to erratic behavior, the stability found for meshes M1 through M4 (in spite of the inherently noisy calculation of the stresses) is encouraging. On the other hand, it is important to realize that the onset of instabilities with mesh refinement observed in traditional flow calculations is marked by the appearance of small wiggles in the velocity profiles, possibly with a periodicity commensurate with grid spacing. The magnitude of these wiggles is well below the size of the error bars in the CONNFFESSIT calculation.

In Figure 13, the statistical error for the 2-D results is displayed as a function of the size of the global ensemble (N_g = 8,192, 32,768, and 65,536). A typical measure for the statistical error was obtained as the standard deviation of the azimuthal velocity at an arbitrarily chosen node (node number 10 at $\theta = 0$, $\xi = 0.6$) of mesh M1 at steady state computed from 25 different runs at each ensemble size. The filled cir-

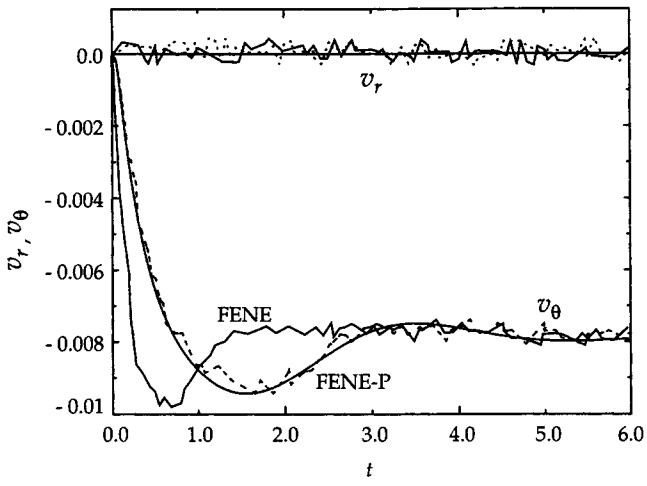

Figure 10. Temporal evolution of azimuthal velocity at $\xi = 0.25$, $\theta = 0$ for FENE (noisy solid line), CONNFFESSIT FENE-P (noisy dashed line), and constitutive equation FENE-P (smooth solid line).

cles represent the magnitude of the velocity fluctuation (one standard deviation) and the error bars the uncertainty in this fluctuation. The line represents the best-fit straight line (weighted least squares), the slope of which in this log-log plot is -0.47 ± 0.02. Although there is no *a-priori* reason for this to be so, the $N_g^{-0.5}$ dependence is very approximately obeyed for the velocity; the same qualitative dependence on N_g was observed at other locations.

Parallelization of the Molecular Simulations

In order to illustrate the suitability of CONNFFESSIT for parallelization, a distributed memory computer (DMC) was chosen for the parallel implementation of a 2-D CONNFFESSIT calculation. The parallelization effort was

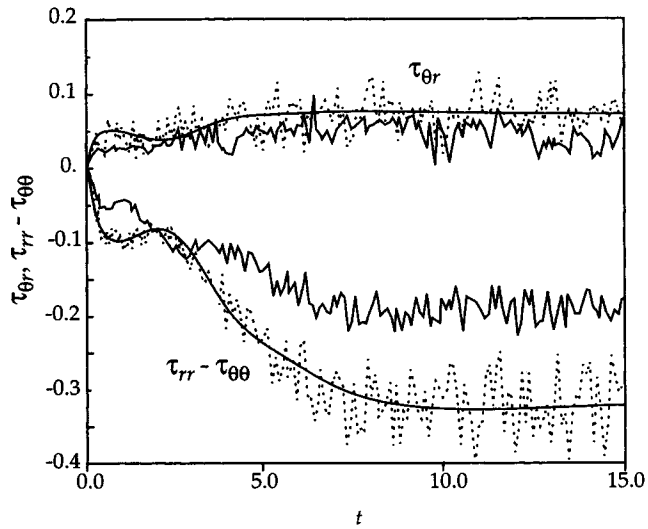

Figure 11. Temporal evolution of stresses at $\xi = 0.25$, $\theta = 0$ for FENE (noisy solid line), CONNFFESSIT FENE-P (noisy dashed line), and constitutive equation (smooth solid line).

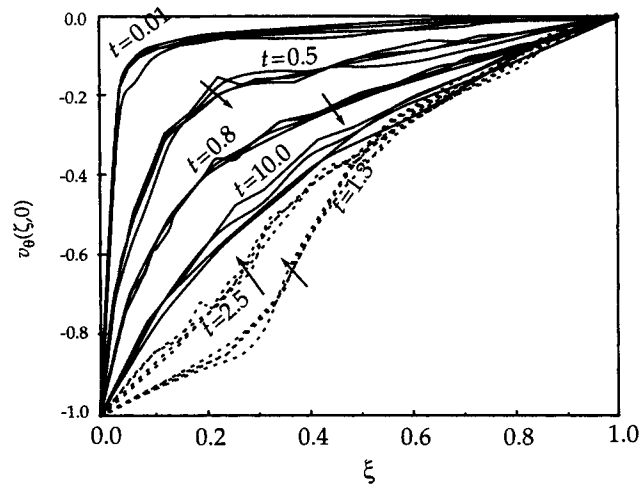

Figure 12. Effect of mesh refinement on radial profile of azimuthal velocity at $\theta = 0$; $\lambda = 3$, $N_g = 2^{19}$ for M1, M2, M3, and M4, and $\epsilon = 0.1$, $\mu = 0.1$, $b = 50$, $\alpha = 0.1$, $\rho = 1$ in all cases.

Arrows indicate direction of advancement of velocity profile. Solid lines correspond to advancing profiles before maximum-velocity overshoot; dashed lines correspond to receding profiles after maximum-velocity overshoot.

concentrated on the molecular (micro) part. No attempt to parallelize the macro routines was made. Parallelization was performed in regard to the element.

The platform selected for the parallel implementation of the 2-D CONNFFESSIT was a Cenju-3 of the Nippon Electric Company (NEC) installed at the Centro Svizzero di Calcolo Scientifico (CSCS). It features 128 nodes with 8 GB of distributed memory and an aggregate peak performance of 6.4 gigaflops. Each of the CPUs is a MIPS-compatible 64-bit VR4400SC RISC processor clocked at 75 MHz and comprising 64 MB main memory, 32 kB of primary cache mounted on chip, and 1 MB of secondary cache. They communicate via a packet-switched multistage interconnection network composed of 4×4 crossbar switches. The Cenju-3 is hosted by one NEC EWS4800, VR4400SC-based Unix workstation,

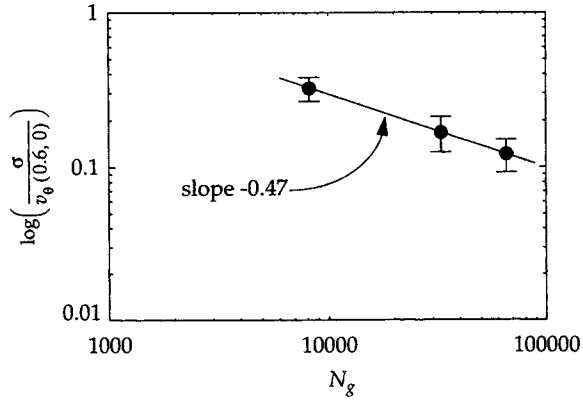

Figure 13. Dependence of the statistical error (one standard deviation) in the velocity on the size of the global ensemble N_g for a fixed mesh (M1) at steady state.

The error bars indicate the uncertainty in the estimated standard deviations; $\mu = 0.1$, $\epsilon = 0.1$, $\alpha = 0.1$, $\rho = 1$.

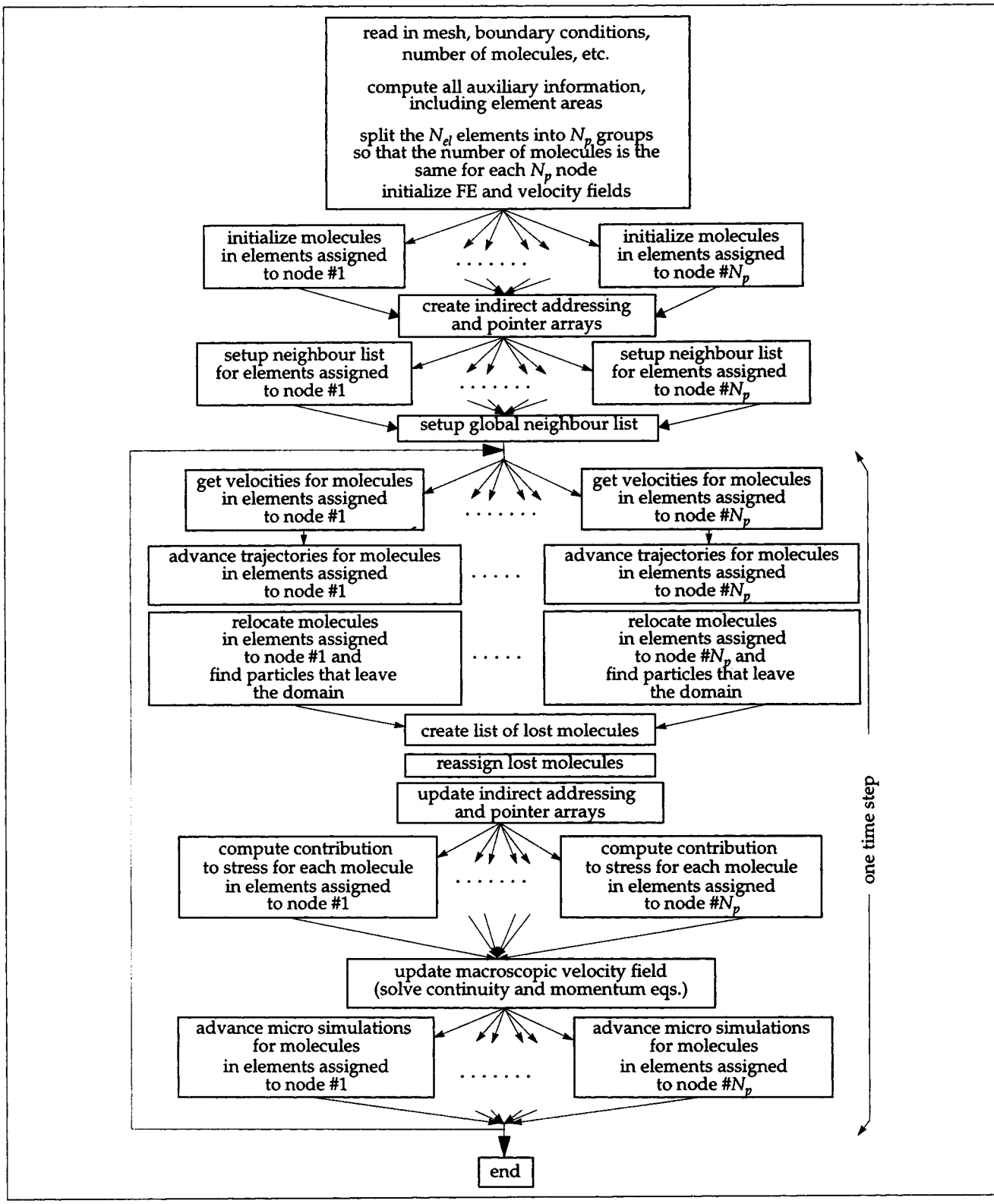

Figure 14. Parallelization scheme.

which is used to log onto the system, to compile and link programs, and to control their execution on partitions of the massively parallel system. Details on the Cenju-3 architecture can be found in Clemençon et al. (1994) and Muramatsu et al. (1995). For parallel programming, a subset of the Message-Passing Interface MPI (MPI Forum, 1994) was used. Additionally, the library PARALIB/CJ from NEC, which allows direct control of transfer between nodes as well as the execution of remote procedure calls, was also available for message passing.

The basic parallelization scheme is presented in Figure 14. The only remaining nonparallel tasks after initialization are those associated with updating the indirect addressing and pointer arrays. Nonparallel tasks are assigned to a single node (or possibly to the host or front-end computer). The remaining nodes are effectively idle during the execution of such tasks. In general this idle time does reduce speedup and efficiency. However, the three single-node tasks in Figure 14 consume only a small fraction of the total time, and therefore do not appreciably affect overall performance unless the number of nodes is very large.

The remaining single-node task (velocity update) can take up a very significant share of the total wall-clock time. Parallelization of the finite-element (macro) computation is a must for good overall performance. For large 2-D or 3-D problems, the effort to be spent in macrocomputations cannot be neglected. Their parallelization is a requirement for good overall performance. Even if the time spent in macrocomputations is as low as 10% of the total on a serial computer, its relative importance starts being appreciable when the microcomputations (consuming 90% of the time on a serial computer) are split among more than $O(10)$ nodes.

While the nonshared tasks could actually be split among several nodes (like the update of the indirect addressing and pointer arrays) by turning to parallel-sorting algorithms (Akl, 1985; Lakshmivarahan et al., 1984), the time consumed by these tasks is comparable to the execution time plus communication overhead of typical parallel schemes for the same task. Thus, complete parallelization of the macrocalculation is not an absolute requirement. It is increasingly less essential the more complicated the microscopic model for the fluid is.

The performance of the parallelization molecular simulations is summarized in Figure 15, which reports calculation times and speedup for eight different hardware configurations with up to 128 nodes. Since only the microcalculations were parallelized, the time spent in the serial finite-element computations is not considered.

Both speedup and efficiency are more than reasonable up to about 16 nodes. A performance analysis showed that two main factors contribute to the decrease in efficiency as the number of nodes increases: first and foremost, as the computation is split among a growing number of nodes, the granularity of individual tasks becomes greater with respect to communication overhead, which grows with the increasing number of nodes; second, the increase in the number of nodes leads to undesirable wait times in calls to synchronization routines (like MPI_BARRIER); in essence, a single stray node can effectively produce a serious deterioration of performance.

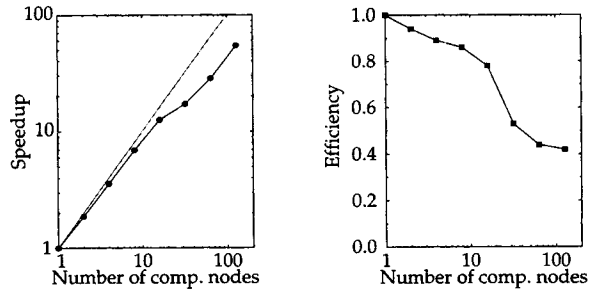

Figure 15. Speedup and efficiency as a function of number of computational nodes.

Mesh M4; 2^{19} particles; 500 time steps.

It is nevertheless remarkable that even for as many as 128 nodes, the efficiency is a sizable 40%, in spite of the relatively simple coding and the asbsence of any load-balancing scheme. In view of the simplicity of the micromodel (noninteracting FENE or FENE-P dumbbells), these efficiency figures are very encouraging. For more complicated molecular models, where the computational nodes spend a proportionally larger fraction of the total time performing the microcalculation, efficiency will be higher. It is also evident that an automatic load-balancing scheme will improve performance: the somewhat jagged aspect of the curve in Figure 15 is partly due to the fact that the number of elements to be distributed among the nodes is not an exact multiple of the number of nodes.

Conclusions

Two-dimensional, time-dependent CONNFFESSIT calculations for the FENE fluid in the journal-bearing geometry have been presented. A number of comparisons with analytical solutions and with continuum-mechanical finite-element calculations show that CONNFFESSIT is (within error bars) a consistent stochastic counterpart of continuum-mechanical approaches. CONNFFESSIT is a viable method for the calculation of viscoelastic flows in complex geometries for molecular models for which no closed-form constitutive equation can be derived. In addition, it can handle effects such as polydispersity, chemical reaction during flow, polymer migration and diffusion, and so forth.

The use of an array sorted with regard to the elements, for the dumbbell indices together with indirect addressing by means of pointer arrays makes it possible to vectorize all manipulations at the molecule level, leading to a performance well in excess of 50% the theoretical peak. As far as parallelization is concerned, the use of indirect addressing and pointing arrays makes elementwise parallelization feasible and efficient. Efficiencies above 40% for 128 nodes can be obtained with relatively unsophisticated parallelization: it is possible to speed up the microcalculation by a factor of 50 using 128 nodes on a commercial platform. The parallelization and vectorization strategies presented are independent of each other; CONNFFESSIT calculations will greatly profit from the coming generation of parallel-vector machines.

In view of the noise level typical of CONNFFESSIT calculations, the implementation of variance reduction techniques is of paramount importance (Melchior and Öttinger, 1996). Such a technique based on Brownian configuration fields has been proposed very recently (Hulsen et al., 1996). This ingenious method is based on the idea of convecting Brownian fields. While being entirely equivalent to CONNFFESSIT, it incorporates an extremely efficient form of variance reduction (for a given computational effort the error bars can be reduced by up to two orders of magnitude). Furthermore, it allows high local spatial resolution. These two features make it vastly superior to the method described in this article whenever efficiency and low statistical noise are essential. "First-generation" CONNFFESSIT will, however, be useful for those tasks where knowledge of the role played by indi-

vidual polymer molecules is relevant (very narrow geometries, singularities, some types of instabilities, etc.). In this sense, both generations of CONNFFESSIT are powerful complementary tools for the investigation of a wide class of flows for complex fluids.

Acknowledgments

The authors are grateful to Pierre Halin and Roland Keunings of the Université Catholique de Louvain for the calculations using the FENE-P constitutive equation. One of the authors (M.L.) wishes to acknowledge funding from the PATI Program of the Spanish Ministry of Energy and Industry. He is also greatly indebted to several members of the staff of the CSCS in Manno for invaluable help with the Cenju-3. Generous allocations of CPU-time on the NEC SX-3 of the CSCS and on the Cray Y-MP of the Rechenzentrum of the ETH are gratefully acknowledged.

Notation

$B(\,)$ = beta function
H = spring constant, N/m
k = Boltzmann's constant, J/K
N_{el} = number of mesh cells or elements
N_p = number of processors
n = number density, m^{-3}
$\boldsymbol{Q}$ = dimensionless or normalized connector vector
R_i = radius of inner cylinder, m
R_o = radius of outer cylinder, m
r = radial coordinate, m
S_R = stress ratio
T = temperature, K
v = velocity, m/s
v_x = x-component of velocity, m/s
v_y = y-component of velocity, m/s
$\boldsymbol{W}$ = 3-D vector of normal random deviates
$\boldsymbol{\delta}$ = unit tensor
$\boldsymbol{\delta}_\alpha$ = unit vector along the α coordinate axis
$\gamma_{(n)}$ = nth rate of strain tensor, s^{-n}
$\overline{\boldsymbol{\kappa}}$ = approximated transposed velocity gradient, s^{-1}
λ_1 = relaxation time constant of Oldroyd-B model, s
λ_2 = retardation time constant of Oldroyd-B model, s
ρ = density, kg/m^3
σ = standard deviation
ζ = friction coefficient, N·s/m

Subscripts

i = time-step index or coefficient index
c = centroid
(n) = nth convected time derivative (codeformational derivative using contravariant components): $\boldsymbol{A}_{(1)} = (\partial/\partial t)\boldsymbol{A} + \{\boldsymbol{v}\cdot\nabla\boldsymbol{A}\} - \{(\nabla\boldsymbol{v})^T\cdot\boldsymbol{A} + \boldsymbol{A}\cdot(\nabla\boldsymbol{v})\}$ $\boldsymbol{A}_{(n)} = (\boldsymbol{A}_{(n-1)})_{(1)}$.

Literature Cited

Akl, S. G., *Parallel Sorting Algorithms*, Academic Press, New York (1985).

Allen, M. P., and D. J. Tildesley, *Computer Simulation of Liquids*, Clarendon, Oxford (1987).

Ballal, B. Y., and R. S. Rivlin, "Flow of a Viscoelastic Fluid Between Eccentric Rotating Cylinders," *Trans. Soc. Rheol.*, **20**, 65 (1976).

Beris, A. N., R. C. Armstrong, and R. A. Brown, "Perturbation Theory for Viscoelastic Fluids between Eccentric Rotating Cylinders," *J. Non-Newtonian Fluid Mech.*, **13**, 109 (1983).

Beris, A. N., R. C. Armstrong, and R. A. Brown, "Finite Element Calculation of Viscoelastic Flow in a Journal Bearing. I: Small Eccentricities," *J. Non-Newtonian Fluid Mech.*, **16**, 141 (1984).

Beris, A. N., R. C. Armstrong, and R. A. Brown, "Finite Element Calculation of Viscoelastic Flow in a Journal Bearing. I: Moderate Eccentricity," *J. Non-Newtonian Fluid Mech.*, **19**, 323 (1986).

Beris, A. N., R. C. Armstrong, and R. A. Brown, "Spectral/Finite Element Calculations of the Flow of a Maxwell Fluid between Eccentric Rotating Cylinders," *J. Non-Newtonian Fluid Mech.*, **22**, 129 (1987).

Bird, R. B., C. F. Curtiss, R. C. Armstrong, and O. Hassager, *Dynamics of Polymeric Liquids*, Vol. II, Wiley, New York (1987).

Burdette, S. R., "Development of the Velocity Field in Transient Shear Flows of Viscoelastic Fluids," *J. Non-Newtonian Fluid Mech.*, **32**, 269 (1989).

Chilcott, M. D., and J. M. Rallison, "Creeping Flow of Dilute Polymer Solutions Past Cylinders and Spheres," *J. Non-Newtonian Fluid Mech.*, **29**, 381 (1988).

Clemençon, C., K. M. Decker, A. Endo, J. Fritscher, N. Masuda, A. Müller, R. Rühl, W. Sawyer, E. de Sturler, B. J. N. Wylie, and F. Zimmermann, "Architecture and Programmability of the NEC Cenju-3," *SPEEDUP J.* (1994).

Davies, M. J., and K. Walters, *Rheology of Lubricants*, T. C. Davenport, ed., Halsted Press (1973).

Feigl, K., M. Laso, and H. C. Öttinger, "A Two-Dimensional Test Problem for the CONNFFESSIT Approach to Solving Viscoelastic Fluid Problems," *Proc. Eur. Rheology Conf.*, C. Gallegos, A. Guerrero, J. Muñoz, and M. Berjano, eds., Sevilla, p. 3261 (1994).

Feigl, K., M. Laso, and H. C. Öttinger, "The CONNFFESSIT Approach for Solving a Two-Dimensional Viscoelastic Fluid Problem," *Macromolecules*, **28**(9) (1995).

Fix, G. J., and P. R. Paslay, "Incompressible Elastic Viscous Lubricants in Continuous-Sleeve Journal Bearing," *J. Appl. Mech. Trans. ASME*, **34**, 579 (1967).

Halin, P., R. Keunings, M. Laso, H. C. Öttinger, and M. Picasso, "Evaluation of a Micro-Macro Computational Technique in Complex Polymer Flows," *Proc. Int. Cong. Rheology*, A. Aït-Kadi, J. M. Dealy, D. F. James, and M. C. Williams, eds., Laval University, Quebec City, Canada, p. 401 (1996).

Herrchen, M., and H. C. Öttinger, "A Detailed Comparison of Various FENE Dumbbell Models," *J. Non-Newtonian Fluid Mech.* (1996).

Hulsen, M. A., A. P. G. van Heel, and B. H. A. A. van den Brule, "Simulation of Viscoelastic Flows Using Brownian Configuration Fields," *J. Non-Newtonian Fluid Mech.* (1996).

Knuth, D. E., *The Art of Computer Programming*, Vol. II, Sec. 3.2, Addison-Wesley, Reading, MA (1981).

Lakshmivarahan, S., S. K. Dhall, and L. L. Miller, *Adv. Comput.*, **23**, 295 (1984).

Laso, M., and H. C. Öttinger, "Calculation of Viscoelastic Flow Using Molecular Models: The CONNFFESSIT Approach," *J. Non-Newtonian Fluid Mech.*, **47**, 1 (1993a).

Laso, M., and H. C. Öttinger, "Von molekularen Modellen zu komplexen Strömungen," *Physik. Blätter*, **49**(2), 121 (1993b).

Lawler, J. V., S. J. Muller, R. A. Brown, and R. C. Armstrong, "Laser Doppler Velocimetry Measurements of Velocity Fields and Transitions in Viscoelastic Fluids," *J. Non-Newtonian Fluid Mech.*, **20**, 51 (1986).

Luo, X. L., and R. I. Tanner, " A Streamline Element Scheme for Solving Viscoelastic Flow Problems. Part II: Integral Constitutive Models," *J. Non-Newtonian Fluid Mech.*, **22**, 61 (1986).

Malkus, D. S., and B. Bernstein, "Flow of a Curtiss-Bird Fluid over a Transverse Slot Using the Finite Element Drift-Function Method," *J. Non-Newtonian Fluid Mech.*, **16**, 77 (1984).

Melchior, M., and H. C. Öttinger, "Variance Reduced Simulations of Polymer Dynamics," *J. Chem. Phys.*, **105**(8), 3316 (1996).

Mochimaru, Y., "Unsteady-State Development of Plane Couette Flow for Viscoelastic Fluids," *J. Non-Newtonian Fluid Mech.*, **12**, 135 (1983).

MPIF, Tech. Rep. CS-94-230, Univ. of Tennessee, Knoxville (1994); also *J. Supercomput. Appl.*, **8** (1994); also available from http://www.mcs.anl.gov/mpi/mpi-report/mpi-report.html.

Muramatsu, K., S. Doi, T. Washio, and T. Nakata, "Implementing a CFD Solver on Cenju-3 Parallel Computer," *Parallel Computational Fluid Dynamics: New Algorithms and Applications*, N. Satofuka and J. Periaux, and A. Ecer, eds., Elsevier, Amsterdam (1995).

Öttinger, H. C., and M. Laso, "Smart Polymers in Finite-Element Calculations," *Theoretical and Applied Rheology, Proc. Int. Congr. on Rheology*, P. Moldenaers and R. Keunings, eds., Elsevier, Brussels (1992).

Öttinger, H. C., "A Model of Dilute Polymer Solutions with Hydrodynamic Interaction and Finite Extensibility. I. Basic Equations

and Series Expansions," *J. Non-Newtonian Fluid Mech.*, **26**, 207 (1987).
Öttinger, H. C., "Incorporation of Polymer Diffusivity and Migration into Constitutive Equations," *Rheol. Acta*, **31**, 14 (1992).
Öttinger, H. C., *Stochastic Processes in Polymeric Fluids*, Springer-Verlag, Berlin (1996).
Öttinger, H. C., and M. Laso, "Bridging the Gap Between Molecular Models and Viscoelastic Flow Calculations," *Lectures on Thermodynamics and Statistical Mechanics*, Chapter VIII, World Scientific, Singapore, p. 139 (1994).
Park, S. K., and K. W. Miller, "Random Number Generators: Good Ones are Hard to Find," *Commun. ACM*, **31**, 1192 (1988).
Peterlin, A., "Einfluss der endlichen Molekülläge auf die Grandientenabhängigkeit des Staudinger-Index," *Makromol. Chem.*, **44–46**, 338 (1961).
Peterlin, A., "Gradientenabhängigkeit der Viskositätszahl in nichtidealen Lösungsmitteln," *Kolloid-Z.*, **182**, 110 (1962).
Phan-Thien, N., and R. I. Tanner, "Journal Lubrication and Normal Stress Measurement," *J. Non-Newtonian Fluid Mech.*, **9**, 107 (1981).
Pironneau, O., *Finite Element Methods for Fluids*, Wiley, New York (1989).
Purnode, B., "Vortices and Change of Type in Contraction Flows of Viscoelastic Fluids," PhD Thesis, Université Catholique de Louvain, Louvain, Belgium (1996).
Rajagopalan, D., J. A. Byars, R. C. Armstrong, and R. S. Brown, "Comparison of Numerical Simulations and Birefringence Measurements in Viscoelastic Flow between Eccentric Rotating Cylinders," *J. Rheol.*, **36**(7), 1349 (1992).
Reiner, M., M. Hanin, and A. Harnoy, "An Analysis of Lubrication with Elastico-Viscous Liquid," *Israel J. Technol.*, **7**, 273 (1969).
Risken, H., *The Fokker-Planck Equation*, Springer Series in Synergetics, Springer-Verlag, Berlin (1989).
Rivlin, R. S., "Some Recent Results on the Flow of Non-Newtonian Fluids," *J. Non-Newtonian Fluid Mech.*, **79**, 79 (1979).
Roberts, G. W., and K. Walters, "On Viscoelastic Effects in Journal-Bearing Lubrication," *Rheol. Acta*, **31**, 55 (1992).
Sommerfeld, A., "Zur hydrodynamischen Thorie der Schmiermittlereibung," *Z. Math. Physik*, **50**, 97 (1904).
Tanner, R. I., "Non-Newtonian Lubrication Theory and Its Application to the Short Journal Bearing," *Aust. J. Appl. Sci.*, **14**, 129 (1963).
van den Brule, B. H. A. A., "Brownian Dynamics Simulation to Finitely Extensible Bead-Spring Chains," *J. Non-Newtonian Fluid Mech.*, **47**, 357 (1993).
Virirayuthakorn, M., and B. Caswell, "Finite Element Simulation of Viscoelastic Flow," *J. Non-Newtonian Fluid Mech.*, **6**, 245 (1980).
Warner, H. R., "Kinetic Theory and Rheology of Dilute Suspensions of Finitely Extensible Dumbbells," *Ind. Eng. Chem. Fundam.*, **11**, 379 (1972).
Wedgewood, L. E., and H. C. Öttinger, "A Model of Dilute Polymer Solutions with Hydrodynamic Interaction and Finite Extensibility: II. Shear Flows," *J. Non-Newtonian Fluid Mech.*, **27**, 245 (1988).
Wedgewood, L. E., D. N. Ostrov, and R. B. Bird, "A Finitely Extensible Bead-Spring Chain Model for Dilute Polymer Solutions," *J. Non-Newtonian Fluid Mech.*, **40**, 119 (1991).
Yeh, P.-W., M. E. Kim-E, R. C. Armstrong, and R. A. Brown, "Multiple Solutions in the Calculation of Axisymmetric Contraction Flow of an Upper Convected Maxwell Fluid," *J. Non-Newtonian Fluid Mech.*, **16**, 173 (1984).
Zone, O., O. Vanderstraeten, and R. Keunings, "A Parallel Direct Solver for Implicit Finite Element Problems Based on Automatic Domain Decomposition," *Massively Parallel Processing: Applications and Development*, L. Dekker, W. Smit, and J. C. Zuidervaart, eds., Elsevier, Amsterdam, p. 809 (1994).

Manuscript received June 10, 1996, and revision received Oct. 18, 1996.